Ocean Sci. Discuss., 8, 1–38, 2011
www.ocean-sci-discuss.net/8/1/2011/
doi:10.5194/osd-8-1-2011

Ocean Science Discussions

Modelling the variability of the Antarctic Slope Current

P. Mathiot[1], H. Goosse[1], T. Fichefet[1], B. Barnier[2], and H. Gallée[3]

[1]TECLIM, Earth and Life Institute, Louvain la Neuve, Belgium
[2]Laboratoire des Ecoulements Géophysiques et Industriels, Grenoble, France
[3]Laboratoire de Glaciologie et Géophysique de l'Environnement, Grenoble, France

Received: 22 December 2010 – Accepted: 23 December 2010 – Published: 11 January 2011

Correspondence to: P. Mathiot (pierre.mathiot@uclouvain.be)

Published by Copernicus Publications on behalf of the European Geosciences Union.

Abstract

One of the main features of the oceanic circulation along Antarctica is the Antarctic Slope Current (ASC). This circumpolar current flows westward and allows communication between the three major basins around Antarctica. The ASC is not very well known due to difficult access and the presence of sea ice during several months, allowing in situ study only during summertime. Moreover, only few numerical studies of this current have been carried out. Here, we investigate the sensitivity of this current to two different atmospheric forcing sets and to four different resolutions in a coupled ocean-sea ice model (NEMO-LIM). Two sets of simulation are conducted. For the first set, global model configurations are run at coarse (2°) to eddy permitting resolutions (0.25°) with the same atmospheric forcing. For the second set, simulations with two different atmospheric forcing sets are performed with a regional circumpolar configuration (south of 30° S) at 0.5° resolution. The first atmospheric forcing set is based on ERA40 reanalysis and CORE data, while the second one is based on a downscaling of the reanalysis ERA40 by the MAR regional atmospheric model.

Sensitivity experiments to resolution show that a minimum model resolution of 0.5° is needed to capture the dynamics of the ASC in term of transport and recirculation. Sensitivity of the ASC to atmospheric forcing fields shows that the wind speed along the Antarctic coast strongly controls the transport and the seasonal cycle of the ASC. An increase of the Easterlies by about 30% leads to an increase of the mean transport of ASC by about 40%. Similar effects are obtained on the seasonal cycle: using a forcing fields with a stronger amplitude of the seasonal cycle leads to double the amplitude of the seasonal cycle of the ASC. To confirm the importance of the wind speed, a simulation, where the seasonal cycle of the wind speed is removed, is carried out. This simulation shows a decrease by more than 50% of the amplitude of the seasonal cycle without changing the mean value of ASC transport.

1 Introduction

The Antarctic Coastal Current (ACoC) or East Wind Drift (Deacon, 1937) is the southernmost current in the world. It flows parallel to the Antarctic coastline and is mainly westwards. Heywood et al. (2004) suggest that the ACoC might be circumpolar, and not be disrupted but the Antarctic Peninsula strongly impedes its flow. In parallel to the ACoC, the Antarctic Slope Front (ASF), described by Whitworth et al. (1998), affects the exchanges of heat, salt and freshwater across the continental shelf, and the transport of water masses around the continent. It is associated with a westward surface-intensified flow, which we refer to here as the Antarctic Slope Current (ASC). The ASF extends continuously from 120° W near the Amundsen Sea westwards to 55° W at the tip of the Antarctic Peninsula (Whitworth et al., 1998). This front is mainly attributed to coastal downwelling caused by the prevailing easterly winds there (Sverdrup, 1953). Heywood et al. (2004) note that the ASC and associated jet are distinctly different from the ACoC (found further south over the continental shelf), although in regions where the continental shelf is narrow, the ACoC and the topographically controlled ASC are sometimes hard to differentiate (Heywood et al., 1998). Thus, in the rest of this paper, all the westward currents flowing around Antarctica (ACoC, ASC and southern branch of polar gyres) are grouped and named Antarctic Slope Current (ASC) for simplicity.

Today, the total westward transport along the Antarctic coast is still debated. For example, across the Princess Elisabeth Trough (PET), Heywood et al. (1999) estimate that the vertically integrated westward transport amounts to 45 Sv, while Bindoff et al. (2000) and Meijer et al. (2010) suggest values of 16 Sv and 28 Sv, respectively. Strong discrepancies are also found along the Antarctic coast of the Australian Antarctic Basin. McCartney and Donohue (2007) estimate the total westward transport to be 76 Sv. This is stronger than the 29 Sv proposed by Bindoff et al. (2000). The seasonal cycle of the total westward transport is also not well known. The recent observational study conducted by Riboni and Fahrbach (2009) along Fimbul Ice Shelf at 0° E suggest that the seasonal cycle of the current velocity is mainly due to the easterly winds. A maximum

current velocity is found during May and June when the easterlies are stronger. Aoki et al. (2010) and Mathiot et al. (2010) in modelling study show also a similar seasonal cycle of the ASC transport.

A better knowledge of the variability of the ASC and of its driving mechanisms, as well as the quantification of the contribution of the driving mechanisms to the variability of this current, would lead to a better understanding of its effects on the biology and physics of the Southern Ocean (e.g., Smedsrud et al., 2006, Rintoul, 2007, Pauly et al., 2000, Heywood et al., 2004). Unfortunately, carrying a ship in this area is expensive and measurements are rather difficult to make because of weather conditions. Satellites are also blinded by presence of sea-ice during nine months and only recent Argo floats can make measurements below sea-ice (Klatt et al., 2007). Thus, the modelling tools can play a major role in improving our knowledge of this area.

In this modelling study, we first evaluate the ability of the European ocean/sea-ice model NEMO (Madec, 2008) to simulate the main characteristics of the ASC, underlining the importance of having a sufficiently high resolution in the ocean and the sensitivity to the forcing field applied. Our second objective is to determine the processes governing the seasonal cycle of the ASC. The paper is organized as follows. Section 2 provides a description of the experimental design. In Sect. 3, we compare the characteristics of the ASC simulated by the model for different resolutions. The response of the ASC to different atmospheric forcing fields is analysed in Sect. 4, sorting out the effect of wind and temperature on annual characteristics and seasonal variability of the ASC. Concluding remarks are finally given in Sect. 5.

2 Experimental design

This section briefly describes the ocean/sea-ice model, the model configurations and the atmospheric forcing fields used.

2.1 Ocean general circulation model

The ocean/sea-ice general circulation model is NEMO (Madec, 2008), the primitive equation free surface ocean model OPA9 coupled to the sea-ice thermodynamic-dynamic model LIM2 (Fichefet and Maqueda, 1997). The surface boundary layer mixing and interior vertical mixing are parameterised according to a turbulent kinetic energy closure model (see the NEMO reference manual, Madec, 2008). The bottom boundary layer parameterisation is based on Beckmann and Döscher (1997). The bottom topography is represented as partial steps. Note that cavities under ice shelves are not represented or parameterized in the model. Bulk formulae provided by Large and Yeager (2004) are used to compute heat and momentum fluxes over the ocean. Over sea ice, the transfer coefficients are fixed to 1.63×10^{-3} for momentum and heat, respectively. In this study, two configurations of NEMO are used: a global one (ORCA) and a regional one (PERIANT).

2.2 Model configurations

2.2.1 ORCA

ORCA is a global configuration of the NEMO model. The nearly isotropic grid resolutions of ORCA configurations (shared by the ocean and sea ice models) used here are 2°, 1°, 0.5° and 0.25° (i.e. 110 km, 55 km, 28 km and 14 km, respectively, at 60° S). The vertical resolution in the ocean comprises 46 levels unequally spaced (6 m in surface and 200 m near the bottom). Initial conditions for temperature and salinity are derived from the Levitus et al. (1998) data set for the low and middle latitudes. For high latitudes, we chose the PHC2.1 climatology (Steele et al. 2001). All the details of the ORCA setup at 0.25° (ORCA025) is given in Barnier et al. (2006). The same characteristics are used for simulations carried out at 2°, 1°, 0.5° and 0.25° resolution.

2.2.2 PERIANT

PERIANT is a regional configuration of NEMO. It is limited to the Southern Ocean and the northern boundary is located at 30° S. Radiative open boundary conditions, inherited from the work of Treguier et al. (2001), are used at the lateral limits of the domain for the oceanic variables.

The initial and open boundary conditions of PERIANT are provided by the 5-day outputs of a global ocean/sea-ice model simulation carried out with the corresponding global ORCA model configuration. The resolution used in this study is 0.5° (22 km at 66° S), and the model setup is the same as the ORCA one.

2.3 Atmospheric forcing fields

Two different forcing sets are used to drive all the ocean/sea-ice circulation model configurations. The first forcing set is the DFS3 one (Brodeau et al., 2010), which was used in hindcasts simulations of the last decades performed with the ORCA025 configuration (Drakkar group, 2007) and with the regional configuration PERIANT (Mathiot et al., 2009). The second forcing set is provided by a dynamical downscaling of ERA40 reanalysis by the regional atmospheric model MAR (Gallée and Schayes, 1994).

2.3.1 DFS3 forcing

The DFS3 forcing combines elements of the CORE (common ocean-ice reference experiments) forcing data set of Large and Yeager (2004) with atmospheric state variables from a 40 Year Re-analysis (ERA40 reanalysis, Simmons and Gibson, 2000). As described in details in Brodeau et al. (2010), the DFS3 atmospheric variables required as forcing by NEMO are (i) from CORE: monthly precipitation rates (rain and snow), daily downward shortwave and longwave radiations, all derived from satellite products, and (ii) from ERA40: 6 hourly 10-m wind speed, air humidity and air temperature (the turbulent fluxes in NEMO are calculated using bulk formulas, Large and Yeager, 2004). The frequencies of DFS3 data are monthly for precipitation, daily for radiation and 6-hourly

for the dynamical variables (i.e. air wind speed, air temperature and air humidity). The spatial resolution is 1.125° for ERA40 data and 1.875° for CORE data. For the simulations conducted with this forcing, all atmospheric data are interpolated on the grid of the corresponding ocean model configuration. Note that, to account for the effects of the katabatic winds around Antarctica, a correction is applied to the original DFS3 forcing. This correction is based on the results obtained with MAR applied over the Antarctic region (see Mathiot et al., 2010) for details.

2.3.2 MAR forcing

The second forcing comes directly from simulations carried out with the MAR model. MAR is a hydrostatic mesoscale atmospheric model based on the three dimensional primitive equations written in terrain following coordinates (Gallée and Schayes, 1994; Gallée, 1995; Gallée et al., 2005). The hydrological cycle includes a cloud microphysical model, with conservation equations for cloud droplet, raindrop, cloud ice crystal and snowflake concentrations. The Antarctic ice sheet is assumed to be entirely covered with snow, and a snow model (Brun et al., 1992) allows snow metamorphism (which affects surface energy fluxes). Blowing snow is also represented in the turbulent scheme (Gallée et al., 2001). The orographic roughness length is derived from the variance of the topography. This length has been tuned with the help of automatic weather station (AWS) data so that valleys in the Transantarctic Mountains are represented as well as possible with regard to the resolution (Jourdain and Gallée, 2010). The tuning of the orographic roughness length is a key point in order to get a good representation of katabatic winds. The grid is a cartesian one on an oblique polar stereographic projection. The horizontal resolution is 40 km and the first vertical level is at ∼10 m. Surface boundary conditions and lateral conditions at the open boundaries of the model domain are from ERA40. MAR is run over a period of twenty years (1980–2000).

Comparison between MAR coastal dynamics and AWS data in some area of Ross sea and along Antarctica has been performed by Mathiot et al. (2010), Jourdain and Gallée (2010) and Petrelli et al. (2008). All these studies show a good agreement

between MAR outputs and AWS data in terms of barrier winds along Transantarctic Mountains and katabatic winds.

As MAR is not global, a merging of all the required atmospheric variables provided by MAR with the fields provided by DFS3 is done. In this application, MAR covers a large part of the Southern Ocean, which includes the whole shelf area and continental slope area around Antarctica. The latitude of this merging is 63° S. As MAR lateral boundary conditions are prescribed from ERA40, a small buffer zone of 2° between DFS3 and MAR forcing fields is applied to smooth the transition and avoid outbreak of unrealistic oceanic features along the merging line.

2.3.3 Comparison of MAR and DFS3 forcings

The major differences between the two forcing fields are the horizontal resolution, the representation of orography and the turbulent scheme in the model used to obtain them. These differences allow a better representation of barrier winds (along TransAntarctic Mountains and along the Antarctic Peninsula) and katabatic winds in MAR. Usually blowing offshore right at the coast, katabatic winds are deflected to the left by the Coriolis force as they move over the ocean (or sea-ice), driving strong easterlies along the coast of Antarctica (Davis and McNider, 1997). As expected, MAR provides katabatic winds stronger than ERA40, and thus stronger easterlies (Mathiot et al., 2010). Easterlies have also a larger seasonal cycle, with weaker winds during summer and stronger winds during autumn in MAR compared to ERA40 (Fig. 1), as observed by Riboni and Farbach (2009). Differences of coastal wind dynamics and turbulence scheme in the MAR model lead to significant changes in surface air temperature along the coast (Fig. 2). Coastal temperatures are lower in MAR, up to −8 °C at 70° S during winter. During summer, differences between MAR and ERA40 temperature are weaker (up to −3°C at 70° S). This lower difference during summer is mainly due to the prescription of the surface temperature to the melting point when sea ice melts. Further details about the differences between MAR with DFS3 forcing fields, see Mathiot et al. (2009).

2.4 Simulations carried out

To study the sensitivity of the ASC to the model resolution and to the atmospheric forcing fields, two sets of simulations are conducted. The first one corresponds to global simulations performed in ORCA configuration within the DRAKKAR project (Drakkar group, 2007) at four resolutions (2° (ORCA2), 1° (ORCA1), 0.5° (ORCA05) and 0.25° (ORCA025)) over the last 50 years (Table 1). All these simulations use the DFS3 forcing fields. The second set of simulations over the period 1980–1989 is done using the regional configuration of the model with a resolution of 0.5° (PERIANT05). In this set of simulations, four experiments (additional to the reference DFS3) are performed. In each experiment, only one component of the forcing is changed (Table 1) and compared to a reference. Comparing DFS3 with WIND simulations (or T10Q10 and MAR) allows studying the sensitivity to the wind forcing. Comparing DFS3 and T10Q10 simulations (or WIND and MAR) gives the sensitivity of ASC to the thermal forcing. In the simulation named SEASO, the climatological (1980–1989) seasonal cycle of the wind forcing provided by MAR is substituted by a climatological annual mean. This simulation is used to diagnose the effects of the seasonal cycle of the wind on the seasonal cycle of ASC. See Table 1 for the details of the set of simulations. In the following part, results about ORCA simulations are averaged over the years 1990–2000. For the PERIANT simulation, the period of study is 1985–1989.

3 Sensitivity of the ASC to model resolution

In this section, we assess the ability of the coarse and high-resolution model configurations to simulate the main features of the ASC. A general overview of the "model performance" in the Southern Ocean area is given in Table 2 for the four configurations. Other studies have analysed in detail the behaviour of ORCA simulations in the southern ocean (Renner et al., 2009; Treguier et al., 2007). Regarding sea ice, all ORCA simulations exhibit the same biases, a lack of sea ice in summer and too large

ice extent during winter. The lack of ice during summer time seems to be due to too warm forcing fields. Simulations T10Q10 and MAR with a colder atmosphere lead as expected to more sea ice in summer. All simulations produce a reasonable transport trough Drake Passage between 115 and 146 Sv against 137 ± 8 Sv in the observations of Cunningham et al. (2003). A comparison of ORCA results with estimates of Klatt et al. (2005) indicates that ORCA2 and ORCA1 underestimate by more than 23 Sv the transport at the southern limb of Weddell Gyre. By contrast, ORCA05 and ORCA025 overestimate this transport by 7 and 14 Sv, respectively.

The ability of the global configurations of the model to simulate the ASC is evaluated along the east coast of Antarctica, from 160° E to 50° E. The coast and the bathymetry of this sector have the particularity to be almost zonal and also well observed during summer by two oceanographic campaigns: BROKE EAST and BROKE WEST (Meijer et al., 2010; Bindoff et al., 2000). Along this coast, the ASC is a continuous current (Meijer et al., 2010; Bindoff et al., 2000), with recirculation along the Kerguelen Plateau (Mac Cartney, 2007).

The zonal transport associated with this current along the Antarctic coast varies significantly between simulations (Fig. 3). ORCA2 has a very weak ASC between 160° E and the Princess Elisabeth Trough (PET, longitude of PET is between 85° E and 80° E). The ASC is blocked by the presence of the PET and is then absent westward of 80° E in the model. In ORCA1, the ASC is better represented. It increases from 2 to 14 Sv between 150° E and 90° E. The PET strongly impedes its flow (−85%). After crossing the PET, the ASC intensifies slowly due to presence of the Weddell Gyre. In these two configurations, PET has a very strong impact on the flow. Clearly, observations do not show such a feature. The ASC is also too weak in ORCA2 and ORCA1. For example, at 110° E, Bindoff et al. (2000) report a total westward transport of 30 Sv, against 1 and 9 Sv in ORCA2 and ORCA1, respectively. At 80° E, a transport of 16 Sv is observed against 0 and 2 Sv, in ORCA2 and ORCA1, respectively.

In ORCA05 and in ORCA025, the total westward transport associated with the ASC is higher, and a significant transport of the ASC is simulated through the PET (Fig. 3).

In ORCA05, the ASC flow increases between 140° E to 90° E from 9 to 25 Sv (gyre recirculation). The recirculation along the Kerguelen Plateau is estimated to be 14 Sv (56% of initial ASC). After crossing the PET, the ASC transport amounts to about 15 Sv. Between 80° E and 60° E, this transport increases and then decreases by 5 Sv. This is the signature of the small Prydz Bay gyre (Nunes Vaz and Lennon, 1996). Afterwards, the ASC enters in the Weddell Gyre. Then, the total westward transport strongly increases after 60° E (+10 Sv between 160° E and 150° E). This description fits well with the one proposed by Bindoff et al. (2000) and Meijers et al. (2010) based on data collected during the oceanographic campaign BROKE. Note that, in ORCA025, the ASC experiences strange features. The increase in transport between 140° E and 90° E has not the same shape as the one simulated by ORCA2, ORCA1 or ORCA05. The ASC does not intensify continuously as in the other simulations. The mean transport in this area is also lower than ORCA05. As far as the PET is concerned, there is no recirculation along the Kerguelen Plateau in ORCA025. All the flow crosses the passage. This feature is characteristic of a large gyre (merge of Weddell Gyre and Australian Antarctic Gyre) instead of two in the observations (Roquet, 2009).

The northward extension of the ASC is in agreement with observations between 160° E and 140° E in all the simulation (Fig. 4). Between 140° E to 50° E, the ASC moves northward in all simulations. Observations show a change in the direction of the current (i.e. from westward to eastward) between 66° S to 64° S and, in models, this point lies between 64° S to 62° S. The ASC in all simulations is too wide before PET. After PET, comparison between observations and model is better, especially for ORCA05 and ORCA025.

Up to now, in the previous part, the description of the ASC was focused on the East coast of Antarctica. A global overview of the ASC is given Fig. 5. In this figure, the four main gyres seen in the observations (Gouretsky, 1999; McCartney and Donohue, 2007; Nunez Vaz and Lennon, 1996; Klatt et al., 2005) are well represented (respectively, the Ross Gyre at 150° W, the Antarctic Australian Gyre at 90° E, the small Prydz Bay Gyre at 75° E and the Weddell Gyre 0° E). A circumpolar feature of the ASC is absent in this

annual description. The presence of the ASC along the West side of the Peninsula is not clear.

The comparison of ORCA2, ORCA1, ORCA05 and ORCA025 results with oceanographic data suggests resolution of 2° and 1° is not enough to simulate the ASC. This resolution is almost the same as the resolution of the climate models used by the IPCC (Randall et al., 2007). We need a resolution of at least 0.5° (about 23 km at 65° S) to catch the main features of ASC. To do relevant processes study, model resolution has to by higher or equal to 0.5°. This resolution of 0.5° is kept in the next session to study the impact of the atmospheric forcing on the ASC.

4 Sensitivity of the ASC to model forcing

In this section, we investigate the influence of the forcing on the simulated ASC. The two forcing fields considered here are quite different but they are both realistic. Given the results discussed in Sect. 3, we use for this study the regional configuration PERI-ANT at 0.5° resolution (Table 1). All the experiments run over 10 years (1980–1989), but only the results of the last 5 years are discussed.

4.1 Effect of different atmospheric variables on the ASC transport

Three different simulations, in addition to the reference simulation DFS3, are performed to determine the effect of the turbulent components of atmospheric forcing fields (see Table 1): wind speed alone (comparison between WIND and DFS3 simulations) and the air temperature and the air humidity (comparison between T10Q10 and DFS3 simulations) and all them together (comparison between MAR and DFS3 simulation). First of all, the main features obtained in these simulations are similar to those present in ORCA05 (see Table 2). However, discrepancies are noticed regarding summer sea ice and the Weddell Gyre transport. As sea ice strongly depend on the atmospheric forcing field, a colder forcing leads to an increase in sea ice extent during summer in

T10Q10 and MAR. During winter, the sea ice extent is almost the same in all simulations (Table 2). However, simulations with MAR lower air temperature induce a thicker sea ice (Mathiot et al., 2009).

Meijers et al. (2010) observed during BROKE WEST, along a section at 60° E across the continental slope, a strong and narrow jet (more than 10 cm/s and 0.2° wide) between the surface and 1000 m with a maximum of 20 cm/s during January. A qualitative comparison shows that all our simulations produce a too wide (about 1°), too slow jet (between 5 cm/s and 10 cm/s). Furthermore, this jet is not deep enough in WIND and MAR simulations (up to 700 m in these simulations), and in T10Q10 and DFS3 simulations (up to 300 m in these simulations), as shown in Fig. 6. During June (maximum of westward transport, discuss later), the jet is deeper, up to 1500 m in simulations carried out with MAR winds (WIND and MAR) and up to 700 m in DFS3 and T10Q10 (Fig. 7). The maximal velocity is also enhanced. In WIND and MAR, a strong jet with velocity higher than 15 cm/s is observed in the first 200 m on the continental slope. In DFS3 and T10Q10, the highest velocity is lower than 15 cm/s. The position of the reverse flow (0 cm/s, white line in Figs. 6 and 7) does not evolve much over the year in all simulations. This limit moves northwards by about only 0.2° (at this latitude, it is only one grid cell). This underlines the strong influence of the forcing fields on both the depth and the velocity of the ASC.

As for the shape of the front, the structure of the ASF is almost the same in all simulations and seasons (Figs. 6 and 7). It is an "I shape" front (following the definition of Bindoff et al., 2000, i.e. the separation of water masses is roughly vertical). In the observations, this shape is observed in many places, especially when a vein of Antarctic Bottom Water (AABW) is absent along the slope (Bindoff et al., 2000). In Meijer et al. (2010), the "I shape" is confirmed at 60° E as in model result. A "V shape" front (following the definition of Bindoff et al., 2000, i.e. the separation of Circumpolar Deep Water, AntArctic Surface water and AntArctic Bottom Water is roughly as a V), observed in some sections in the observations, couldn't be found in our simulations. It is due to the excessive mixing of High Salinity Shelf Water along the continental slope

in z vertical coordinates model (Griffies et al., 2000), which inhibits the formation of AABW along the slope. The front in PERIANT05 is also too wide, about 0.5° in latitude. During the BROKE campaign, between 80° E and 150° E and between 30° E and 80° E, the width of ASC front observed is between 0.1° to 0.2°.

In Fig. 8, we present the location where 13 different sections through which the annual integrated transport of the ASC is calculated. Values of this transport are given in Fig. 8. Each section extends from the coast to the bathymetry line 3500 m. As show in Figs. 4, 6 and 7, this northern limit of the sections allows to capture almost the entire ASC vein during all seasons (in January for the minimum and in June for the maximum). This boundary also avoids capturing part of the ACC transport in some simulations. However, with this method, the parts of the ASC, which is flowing north of the bathymetry line 3500 m, are missing in our transport. The sections are distributed all along Antarctica from west side of the Antarctic Peninsula (section #1) to Bransfield Straight at the tip of the Antarctic Peninsula (section #13). Along the west side of the Antarctic Peninsula (section #1), the presence of an ASC is not clear in all simulations carried out. This is also the case in the observation collected by Martinson et al. (2008). Between Bellingshausen and Amundsen Seas (section #2), a weak westward flow is observed only in the DFS3 and WIND simulations. This flow increases in magnitude from the Bellingshausen Sea to the Amundsen Sea (section #3) as in Holland et al. (2010).

In all the simulations, the ASC strengthens strongly after having passed the Ross Sea. Transport of ASC across the through between Baleny Island and the Antarctic continent (section #4 in Fig. 9) has a transport ranging between 11 Sv (T10Q10 simulation) and 16 (WIND simulation) compared to 3 Sv at the entrance of the Ross Sea at 150° W. Up to the PET, the strength of the ASC remains almost constant. A decrease of 5 Sv is then observed after the ASC crosses the PET (section #9 in Fig. 9). This decrease is due to the recirculation along the Kerguelen Plateau (McCartney and Donohue, 2007) as shown for ORCA05. After crossing PET, the ASC intensifies slowly up to the entrance of the Weddell Sea near Brunt Ice Shelf. The ASC transport strongly

increases along the Antarctic Peninsula (section #12 in Fig. 9). After section 12, almost all the flow turns east in the ACC and in the Weddell Gyre. A small part (less than 1 Sv) turns west across the Bransfield Straight at the tip of Antarctic Peninsula (Fig. 9) as suggested by Heywood et al. (2004) and Von Gyldenfeldt et al. (2002).

All sections show a stronger ASC transport in simulations done with MAR wind (WIND and MAR) compared to the similar simulations done with DFS3 wind (DFS3 and T10Q10). On the other hand, the ASC is weaker everywhere in simulations done with MAR temperature and humidity (T10Q10 and MAR) compared to the similar simulations done with DFS3 temperature and humidity (DFS3 and WIND). The increase in ASC transport due to the MAR winds is about 40% along all the east coast of Antarctica, the decrease caused by temperature being less than 10% in the same area. This suggests that the wind is the most important atmospheric variable controlling the ASC transport between the surface and 2000 m.

4.2 Wind forcing of the seasonal cycle of the ASC

Up to now, we have confirmed that the annual ASC transport is strongly influenced by the wind speed. As MAR and ERA40 winds have different seasonal cycles (see Fig. 1), the question now is: how the seasonal cycle of the wind affects the seasonal cycle of the transport associated with the ASC?

To answer this question, we first analyse the seasonal cycle of the transport at the sections presented in Fig. 8. The results are displayed for both WIND and DFS3 simulations (which only differ by the wind forcing) in Fig. 10.

This figure indicates that, in both simulations, the ASC transport has a strong seasonal cycle at all sections. Maximum transport is reached in May and minimum occurs in summer (December, January or February) as suggested by the observations of Riboni et al. (2009) along the Fimbul ice-shelf. As expected, the stronger easterlies in the MAR forcing lead to a seasonal cycle of the ASC transport of larger amplitude (Fig. 10) along all the Antarctic coasts, especially along the east coast and in Weddell Sea. In these areas, the amplitude of the seasonal cycle is larger by at least 5 Sv in WIND

than in DFS3. In other words, this amplitude is doubled when using the MAR wind fields. Figure 10 also shows that, during summer time, the flow along the west coast of Antarctic Peninsula and in the Bellingshausen Sea becomes eastwards in the WIND and DFS3 simulations. The transport in this area is strongly increased between March and September when MAR winds is used, compared to DFS3 (up to 80% during July).

To confirm the strong impact of the seasonality of the wind forcing on the seasonal cycle of the ASC, a comparison between MAR and SEASO simulations is performed. SEASO is the same simulation as MAR, but the seasonal cycle of each wind component over the period 1980–1989 is removed, the model being driven by the annual mean value of the wind speed component over the same period. Figure 11 reveals that the absence of seasonal cycle leads to a decrease in the amplitude of the ASC seasonal cycle of the transport, in all sections, by at least 50%.

A small residual seasonal cycle is however still present (from 1 to 2 Sv). This feature could be caused by the seasonal variations of (1) the drag coefficient used to compute wind stress and the heat fluxes over the ocean, (2) the presence of sea ice coverage and (3) the water mass properties on the continental shelf and slope.

This strong sensitivity to wind of the ASC seems to be a direct effect of change in sea surface height along Antarctic coast via Ekman drift. Sea Surface Height (SSH) along the Antarctic coast is higher in simulation with stronger Easterlies (MAR and WIND), and almost the same in open ocean (north of 63° S for the East coast) as show in Fig. 12. This leads to a higher pressure gradient between coast and open ocean in WIND (or MAR) than in DFS3 (or T10Q10). As a consequence, the transport of ASC is higher in WIND (or MAR) simulations than in DFS3 (or T10Q10) simulations.

Almost the same feature is observed between January and May (Fig. 13a). In January, SSH along the coast is lower than in May. In the open ocean, SSH is higher in January than in May. Thus the pressure gradient is lower during January. This lower pressure gradient in January between coast and open ocean inhibits the presence of a powerful ASC. As expected in SEASO (Fig. 13b), the SSH gradient difference between coastal area and open ocean between January and May are low compare to

MAR simulation (Fig. 13a). To sum up, the effect of wind on the ASC seems to be due to a change of the SSH gradient via a direct effect of Ekman drift, and this holds for the seasonal cycle of the amplitude of the ASC and also for the difference of transport observed in the simulations carried out.

5 Conclusions

The main goal of this study was to investigate the sensitivity of the ASC to different model characteristics such as the resolution and atmospheric forcing, with a focus on the influence of wind on the seasonal cycle of the ASC. A hierarchy of model configurations (2°, 1°, 0.5° and 0.25° of resolution) set up by the DRAKKAR project were tested. All the conducted simulations were run over the last 50 years with the same experimental design. To evaluate the realism of those simulations, general diagnostics were made. These concerned Antarctic sea ice and the transport through the Drake Passage and in the Weddell Gyre. The modelled coastal westward transport was also thoroughly examined. The resolution does not seem to impact the sea ice extent, both in summer and winter. In summer time, the sea ice coverage computed by the model is largely underestimated in all cases. During winter, a slight overestimation of sea ice extent is simulated. Regarding the transport through the Drake Passage, all the simulations are realistic (from 146 to 115 Sv in the model against 136 ± 8 Sv in the observations). In the southern branch of Weddell gyre, low-resolution models (ORCA2 and ORCA1) yield a mean transport of 25 and 33 Sv, respectively, and the high-resolution models (ORCA05 and ORCA025) simulate a mean transport with a transport of 63 to 70 Sv, respectively, while observations give 56 ± 8 Sv. A detailed analysis of the model dynamics along East Antarctica coasts revealed that the ASC transport in ORCA2 is not continuous at Princess Elisabeth Though (PET). In ORCA1, PET strongly impedes the ASC flow (only 1 Sv remains after PET). In ORCA025, there is no recirculation along the Kerguelen Plateau, due to (wide) Weddell Australian Antarctic Gyre in the model. This wide gyre is unrealistic, but the westward transport along the coastline is

in agreement with observational estimates. In ORCA05, the ASC transport in the vicinity of the PET is realistic, and the presence of the small Prydz Bay gyre is simulated. ORCA05 show better realism in terms of representation of gyre dynamics and coastal dynamics. Thus, the rest of our study was done with a southern regional configuration of the model based on ORCA05 (PERIANT05).

In order to indentify the role played by each forcing component in the ASC dynamics, five simulations were performed: four to test the effect of wind speed and air temperature, and another one to test the effect of the seasonality of the wind. All simulations were carried out over the period 1980–1989. Two forcing fields were used. The first one is DFS3. Turbulent variables (wind, temperature and humidity) were derived from ERA40 reanalysis. The second one (MAR) was built from results of a regional atmospheric model applied over the Antarctic regions. The MAR easterlies are ± 30% stronger than the DFS3 ones and they also have a larger seasonal cycle. Surface temperatures are also lower in the MAR forcing compared to the DFS3 one (−4° at 66° S). The impacts of these differences on the model behaviour are diagnosed around Antarctica. Two changes are observed. One is the deepening of the ASC vein when the wind increases. With MAR wind the ASC vein reach 1500 m instead of 700 m with the DFS3 wind. The other one is the increase in the total westward transport along the Antarctic coasts when the wind increases (+5 Sv between WIND and DFS3). Along the west side of the Antarctic Peninsula and in the Bellingshausen and Amundsen Seas changes are not large in absolute value (less than 1 Sv), but, in relative value, they can reach 100%. A detailed comparison between the WIND and DFS3 simulations indicated that the minimum and maximum of the seasonal cycle of the ASC transport in those two simulations occur in the same month in all sections considered in this study: this current is weak in January and strong in June. However, the amplitude of the seasonal cycle of ASC transport is different: 10 Sv along the east coast of Antarctica in WIND and 5 Sv in DFS3. A final simulation without seasonal cycle of wind (SEASO) shows that more than 50% of the amplitude of the seasonal cycle of the ASC transport is due to the wind seasonal cycle.

Acknowledgement. The authors acknowledge support from the Ministère de l'Education Nationale et de la Recherche and from Centre National de la Recherche Scientifique (CNRS). This work is a contribution of the DRAKKAR project. Support to DRAKKAR comes from various grants and programs listed hereafter: French national programs GMMC, LEFE, and PICS2475. The contribution of Institut National des Sciences de l'Univers (INSU) to these programmes is particularly acknowledged. DRAKKAR acknowledge the support from the Centre National d'Etudes Spatiales (CNES) through the OST/ST. Computations presented in this study were performed at Institut du Développement et des Ressources en Informatique Scientifique (IDRIS), Paris. Partial support from the European Commission under Contract SIP3-CT-2003-502885 (MERSEA project) is gratefully acknowledged. H. Goosse is Research Associate with the Fonds National de la Recherche Scientifique (F.R.S. – FNRS-Belgium). This work is also partly supported by the F.R.S. – FNRS, the Belgian Federal Science Policy Office, Research Program on Science for a Sustainable Development, and the Fonds Special de la Recherche of the Université Catholique de Louvain.

References

Aoki, S., Sasai, Y., Sasaki, H., Mitsudera, H., and Williams, G. D.: The cyclonic circulation in the Australian-Antarctic basin simulated by an eddy-resolving general circulation model, Ocean Dynam., 60, 743–757, doi:10.1007/s10236-009-0261, 2010.

Barnier, B., Madec, G., Penduff, T., Molines, J.-M., Treguier, A.-M., Le Sommer, J., Beckmann, A., Biastoch, A., Böning, C., Dengg, J., Derval, C., Durand, E., Gulev, S., Remy, E., Talandier, C., Theeten, S., Maltrud, M., McClean, J., and De Cuevas, B.: Impact of partial steps and momentum advection schemes in a global ocean circulation model at eddy-permitting resolution, Ocean Dynam., 56, 543–567, 2006.

Beckmann, A. and Doesher, R.: A method for improved representation of dense water spreading over topography in geopotential-coordinate models, J. Phys. Oceanogr., 27, 581–591, 1997.

Bindoff, N. L., Rosenberg, M. A., and Warner, M. J.: On the circulation and water masses over the Antarctic continental slope and rise between 80 and 150° E, Deep-Sea Res. Pt. II, 47, 2299–2326, 2000.

Brodeau, L., Barnier, B., Penduff, T., Treguier, A.-M., and Gulev, S.: An ERA40 based atmospheric forcing for global ocean circulation models, Ocean Model., 31, 88–104, 2010.

Brun, E., David, P., Sudul, M., and Brunot, G.: A numerical model to simulate snow cover stratigraphy for operational avalanche forecasting, J. Glaciol., 128, 13–22, 1992.

Cunningham, S., Alderson, S., King, B., and Brandon, M.: Transport and variability of the Antarctic circumpolar current in Drake Passage, J. Geophys. Res., 108, C05, 2003.

Davis, A. M. J. and McNider, R. T.: The development of Antarctic Katabatic Winds and implications for the Coastal Ocean, J. Atmos. Sci., 54, 1248–1261, 1997.

Deacon, G.: The hydrology of the Southern Ocean. Discovery Rep. 15, Institute of Oceanography Science, Southampton UK, 3–122, 1937.

DRAKKAR-Group: Eddy permiting ocean circulation hindcast of past decades, CLIVAR Exch. Lett., 12, 8–10, 2007.

Fichefet, T. and Morales Maqueda, M. A.: Sensitivity of a global sea ice model to the treatment of ice thermodynamics and dynamics, J. Geophys. Res., 102, 12609–12646, 1997.

Fetterer, F. and Knowles, K.: Sea ice index monitors polar ice extent, Eos Trans., AGU, 16, 2004.

Gallée, H.: Simulation of the mesocyclonic Activity in the Ross Sea, Antarctica, Mon. Weather Rev., 123, 2050–2069, 1995.

Gallée, H. and Schayes, G.: Development of a three dimensional meso-scale primitive equations model, katabatic winds simulation in the area of Terra Nova Bay, Ant. Mon. Weather Rev., 122, 671–685, 1994.

Gallée, H., Guyomarc'h, G., and Brun, E.: Impact of snow drift on the antarctic ice sheet surface mass balance: possible sensitivity to snow-surface properties, Bound.-Lay. Meteorol., 99, 1–19, 2001.

Gallée H., Peyaud, V., and Goodwin I.: Simulation of the net snow accumulation along the Wilkes Land transect, Antarctica, with a regional climate model, Ann. Glaciol., 41, 1–6, 2005.

Gouretsky, V.: The large-scale thermohaline structure of the Ross Gyre. Oceanography of the Ross Sea, Antarctica. Springer, Berlin, 77–100, 1999.

Griffies, S. M., Böning, C., Bryan, F. O., Chassignet, E. P., Gerdes, R., Hasumi, H., Hirst, A., Treguier, A.-M., and Webb, D.: Developments in ocean climate modeling, Ocean Model., 2, 123–192, 2000.

Heywood, K. J., Locarnini, R., Frew, R., Dennis, P., and King, B.: Transport and water masses of the Antarctic slope front system in the Eastern Weddell Gyre. Ocean, Ice and Atmosphere:

Interactions at the Antarctic Continental Margin, Antarctic Research Series, American Geophysical Union, Washington, 75, 203–214, 1998.
Heywood, K., Sparrow, M., Brown, J., and Dickson, R.: Frontal structures and antarctic bottom water flow through the Princess Elizabeth trough, Antarctica, Deep-Sea Res. Pt. I, 46, 7, 1181–1200, 1999.
Heywood, K. J. and Navaira Garabato, A. C.: On the fate of the Antarctic Slope Front and the origin of the Weddell Front, J. Geophys. Res., 109, C06021, 2004.
Holland, P. R., Jenkins, A., and Holland, D. M.: Ice and ocean processes in the Bellingshausen Sea, Antarctica, J. Geophys. Res., 115, C05020, doi:10.1029/2008JC005219, 2010.
Jourdain, N. C., and Gallée, H.: Influence of the representation of glacier valleys across the Transantarctic Mountains in an atmospheric regional model, Climate Dynam., doi:10.1007/s00382-010-0757-7, 2010.
Klatt, O., Fahrbach, E., Hoppema, M., and Rohardt, G.: The transport of the Weddell Gyre across the Prime Meridian, Deep-Sea Res. Pt. II, 52, 513–528, 2005.
Klatt, O., Boebel, O., and Farhbach, E.: A profiling float's sense of ice, J. Atmos. Ocean. Technol., 24, 1301–1308, 2007.
Large, W. G. and Yeager, S. G.: Diurnal to decadal global forcing for ocean and sea-ice models: The data sets and flux climatologies. Technical Report TN-460+STR, NCAR, 105pp, 2004.
Levitus, S., Boyer, T. P., Conkright, M. E., O'Brian, T., Antonov, J., Stephens, C., Stathopolos, L., Johnson, D., and Gelfeld, R.: World ocean database 1998. NOAA Atlas NESDID 18, US Government Printing Office, Washington, DC, 1998.
Madec, G.: The NEMO ocean engine, Note du Pôle de Modlisation de L'IPSL, available at: http://www.nemo-ocean.eu/About-NEMO/Reference-manuals, 2008.
Martinson, D. G., Stammerjohn, S. E., Iannuzzi, R. A., Smith, R. C., and Vernet, R. C.: Western Antarctic Peninsula physical oceanography and spatio-temporal variability, Deep-Sea Res. Pt. II, 55, 1964–1987, 2008.
Mathiot, P.: Influence du forage atmosphérique sur la représentation de la glace de mer et des eaux de plateau en Antarctique dans une étude de modélisation numérique, Phd thesis, Université Joseph Fourier, available at: http://tel.archives-ouvertes.fr/tel-00375960, 2009.
Mathiot, P., Barnier, B., Gallée, G., Molines, J. M., Le Sommer, J., Juza, M., and Penduff, P.: Introducing katabatic winds in global ERA40 fields to simulate their impacts on the Southern Ocean and sea-ice, Ocean Model., 35, 3, 119–216, 2010.
McCartney, M. S. and Donohue, K. A.: A deep cyclonic gyre in the Australian–Antarctic Basin,

Progress Oceanogr., 75, 675–750, 2007.
Meijers, A. J. S., Klocker, A., Bindoff, N. L., Williams, G. D., and Marsland, S. J.: The circulation and water masses of the Antarctic shelf and continental slope between 30° E and 80° E, Deep-Sea Res. Pt. II, 57, 723–737, 2010.
Nunes Vaz, R. A. and Lennon, G. W.: Physical oceanography of the Prydz Bay region of Antarctic waters, Deep-Sea Res. Pt. I, 43, 5, 603–641, 1996.
Pauly, T., Nicol, S., Higginbottom, I., Hosie, G., and Kitchener, J.: Distribution and abundance of Antarctic krill (*Euphausia superba*) off East Antarctica (80–150° E) during the Austral summer of 1995/1996, Deep-Sea Res. Pt. II, 47, 2465–2488, 2000.
Petrelli, P., Bindoff, N. L., and Bergamasco, A.: The sea ice dynamics of Terra Nova Bay and Ross Ice Shelf Polynyas during a spring and winter simulation, J. Geophys. Res., 113, C09, 2008.
Randall, D. A., Wood, R. A., Bony, S., Colman, R., Fichefet, T., Fyfe, J., Kattsov, V., Pitman, A., Shukla, J., Srinivasan, J., Stouffer, R. J., Sumi, A. and Taylor, K. E.: Climate models and their evaluation, in: Climate Change 2007: The Physical Science Basis. Contribution of Working Group I to the Fourth Assessment Report of the Intergovernmental Panel on Climate Change, edited by: Solomon, S., Qin, D., Manning, M., Chen, Z., Marquis, M., Averyt, K. B., Tignor, M., and Miller, H. L., Cambridge University Press, Cambridge, United Kingdom and New York, NY, USA, 2007.
Renner, A. H. H., Heywood, K. J., and Thorpe, S. E.: Validation of three global ocean models in the Weddell Sea, Ocean Model., 30, 1–15, 2009.
Riboni, I. N. and Fahrbach, E.: Seasonal variability of the Antarctic Coastal Current and its driving mechanisms in the Weddell Sea, Deep-Sea Res. Pt. I, 56, 1927–1941, 2009.
Rintoul, S. R.: Rapid freshening of Antarctica Bottom Water formed in the Indian and Pacific oceans, Geophys. Res. Lett., 34, L06606, doi:10.1029/2006GL028550, 2007.
Roquet, F.: La circulation océanique autour du plateau de Kerguelen: De l'observation à la modélisation. Phd thesis, Université Pierre et Marie Curie, available at: http://tel.archives-ouvertes.fr/tel-00431483/, 2009.
Simmons, A. J., and Gibson, J. K.: The era-40 project plan. Technical report, ERA-40 project report series, 2000.
Steele, M., Morley, R., and Ermold, W.: PHC: a global ocean hydrography with a high quality Arctic Ocean, J. Climate, 14, 2079–2087, 2001.
Smedsrud, L. H., Jenkins, A., Holland, D. M., and Nost, O. A.: Modeling ocean processes below

Fimbulisen, Antarctica, J. Geophys. Res., 111, C01007, 1–14, 2006.
Sverdrup, H. U.: The currents off the coast of Queen Maud Land, Nor. Geogr. Tidsskr., 14, 239–249, 1953.
Treguier, A.-M., Barnier, B., de Miranda, A., Molines, J.-M., Grima, N., Imbard, M., Madec, G., Messager, C., and Michel, S.: An eddy permitting model of the Atlantic circulation: evaluating open boundary conditions, J. Geophys. Res., 106, 22115–11129, 2001.
Treguier, A. M., England, M. H., Rintoul, S. R., Madec, G., Le Sommer, J., and Molines, J.-M.: Southern Ocean overturning across streamlines in an eddying simulation of the Antarctic Circumpolar Current, Ocean Sci., 3, 491–507, doi:10.5194/os-3-491-2007, 2007.
Von Gyldenfeldt, A.-B., Fahrbach, E., Garcia, M. A., and Schroder, M.: Flow variability at the tip of the Antarctic Peninsula, Deep-Sea Res. Pt. II, 49, 4743–4766, 2002.
Whitworth III, T., Orsi, A. H., Kim, S. J., Nowlin, W. D., and Locarmini, R. A.: Water masses and mixing near the Antarctic Slope Front. Ocean, ice and atmosphere, Antarct. Res. Ser., 75, 1998.

Table 1. Simulation description (resolution, forcing and configuration).

	Configuration	Resolution	Wind forcing	Air temp. forcing
ORCA2	ORCA	2°	DFS3	DFS3
ORCA1	“	1°	“	“
ORCA05	“	0.5°	“	“
ORCA025	“	0.25°	“	“
DFS3	PERIANT	0.5°	DFS3	DFS3
WIND	“	“	MAR	DFS3
T10Q10	“	“	DFS3	MAR
MAR	“	“	MAR	MAR
SEASO	“	“	MAR – seasonal cycle	MAR

Table 2. Ice extent, transport through Drake Passage and transport in Weddell Gyre along the Greenwich Meridian for all simulations (period 1990–2000). The definition of the sea-ice extent used here is the area where sea-ice concentration is greater than 15%. Observations come from Fetterer and Knowles (2004) (SSMI data) for sea-ice extent, Cunningham et al. (2003) for transport through Drake Passage and from Klatt et al. (2005) for the transport in the Weddell Gyre along the Greenwich Meridian.

Simulation	Sea ice extent (million km^2)		Transport across	Transport of
	February	September	Drake passage (Sv)	Weddell Gyre (Sv)
ORCA2	1.0	19.0	142	25
ORCA1	1.6	21.4	146	33
ORCA05	0.3	20.2	127	63
ORCA025	0.4	20.4	115	70
DFS3	1.1	20.2	130	63
T10Q10	5.0	20.5	132	61
WIND	1.2	20.2	125	70
MAR	4.4	20.5	126	68
Observations	2.9	18.8	137 ± 8	56 ± 8

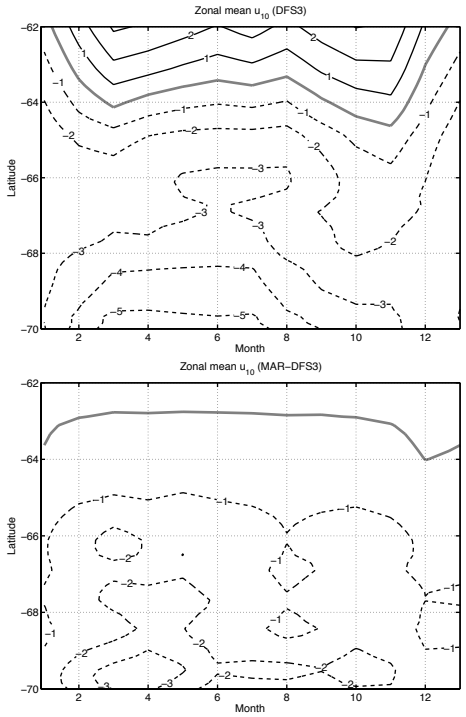

Fig. 1. Zonal mean (0° E–150° E) of the zonal component of the wind speed (u_{10}) between 1980–1989 in DFS3 (top) and of the zonal mean difference of the u_{10} between MAR and DFS3 (bottom). In the upper figure, black line corresponds to a westerly wind and black dash line to an easterly wind. In the lower figure, a black dashed line corresponds to a stronger easterlies wind in MAR and the thick grey line corresponds to the 0 difference line.

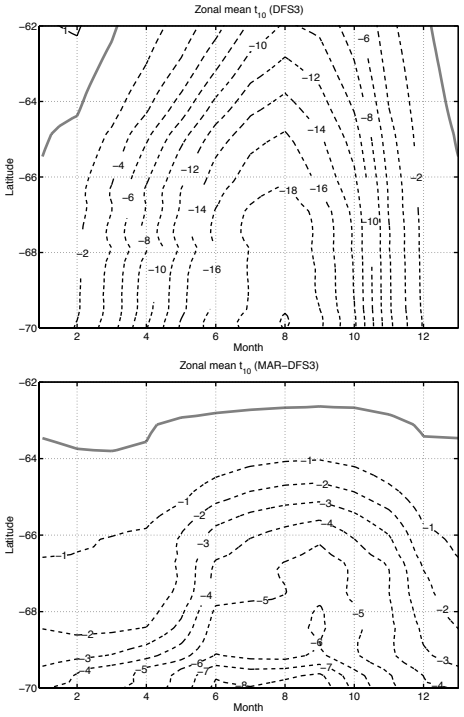

Fig. 2. Zonal mean (0° E–150° E) of the air temperature (t_{10}) between 1980–1989 in DFS3 (top) and of the zonal mean difference of the t_{10} between MAR and DFS3 (bottom). Top: the thick grey line is the isotherm 0 °C. Bottom: the thick grey line is the 0 line, and negative values (dash lines) mean a colder atmosphere in MAR.

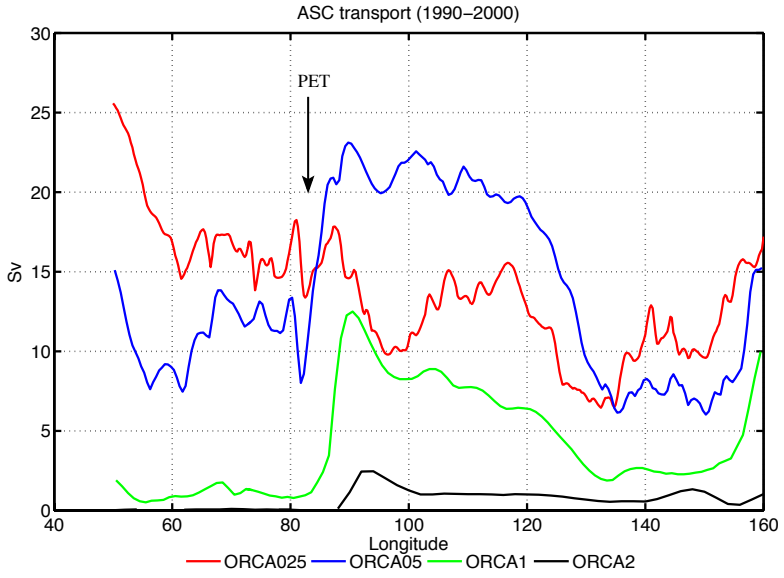

Fig. 3. Maximum cumulated westward transport from the coast to 62° S between 50° E to 160° E during February. Choice of 62° S has been done to avoid stationary eddies in the ACC (in ORCA025) and recirculation along bathymetry features like the Kerguelen Plateau. Each colours (red, blue, green and black) corresponding, respectively to one resolution (ORCA025, ORCA05, ORCA1 and ORCA2). ASC flow come in at 160° E (right side of the plot) and come out at 50° E (left side of the plot). "PET" corresponds with the location of the Princess Elisabeth Trough.

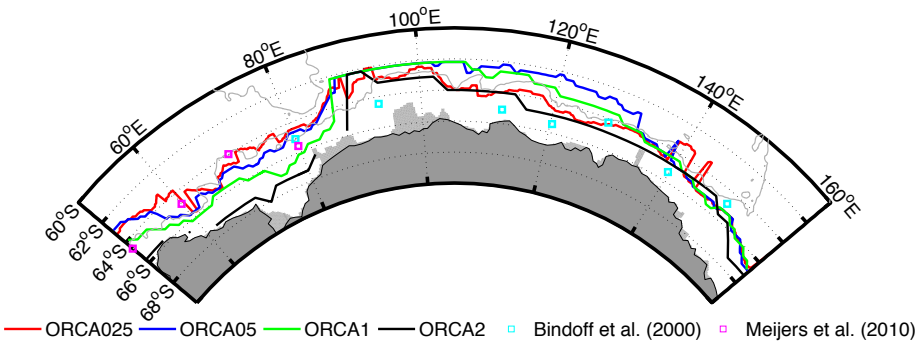

Fig. 4. Position of the maximum cumulated westward transport of the ASC along the East Antarctic coast between 50° E to 160° E calculated in Fig. 3. The grey line is the bathymetry line 3500 m. The colour code used is the same as in Fig. 3. The cyan and magenta squares correspond to the positions of the maximum cumulated westward transport in the observations of respectively, Bindoff et al. (2000) and Meijers et al. (2010). Presence of pics at 142° E and 60° E is due to presence of eddy or filament in the model.

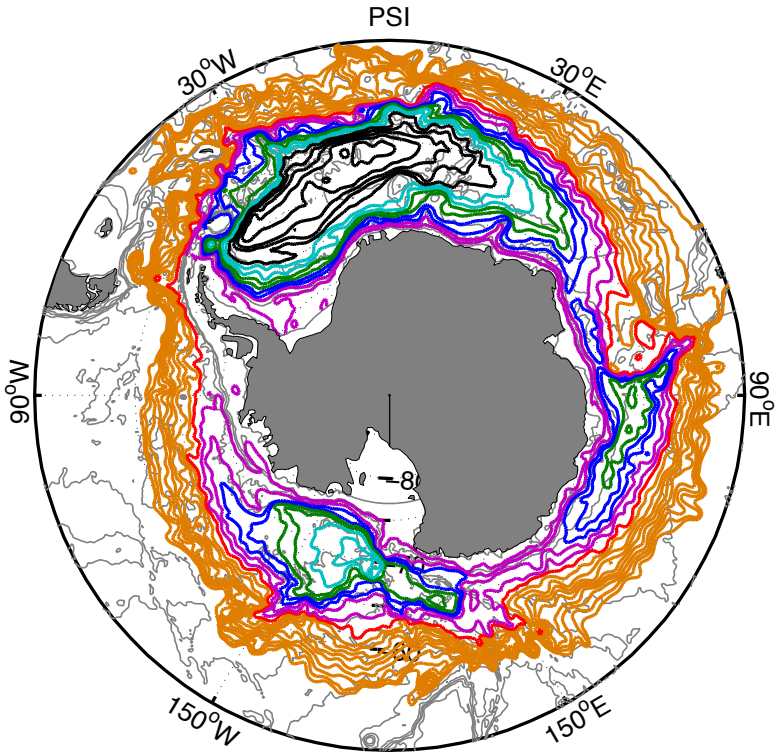

Fig. 5. Map of annual stream line in the southern ocean in ORCA05 simulation. Step between two lines is 5 Sv. The ASC is defined here by the southern part of the gyres and the magenta lines. Gray lines corresponding to bathymetry line each 1000 m.

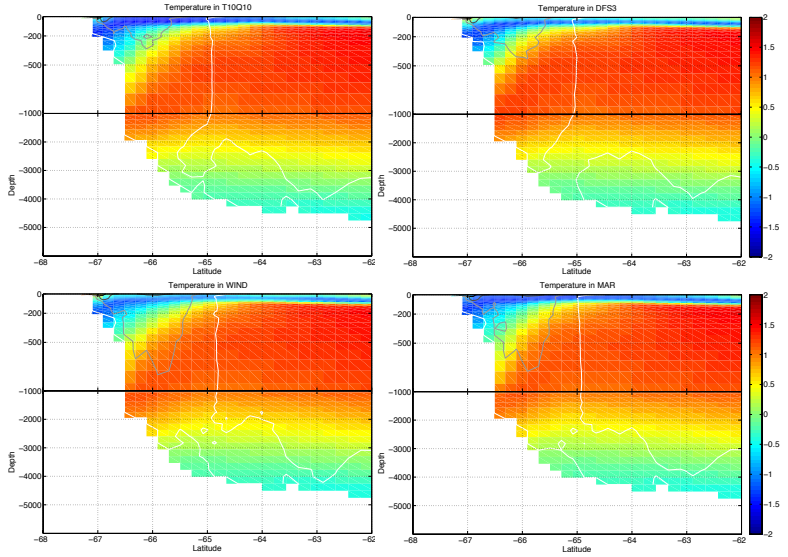

Fig. 6. Section at 60° E in simulations T10Q10, DFS3, WIND and MAR during January. Temperature is in colour and zonal currents are represented by solid lines (white is 0 cm/s, light grey is 5 cm/s, dark grey line is 10 cm/s). The white area corresponds to the ocean floor. Notice that the vertical scale is not linear; a zoom is done on the first 1000 m.

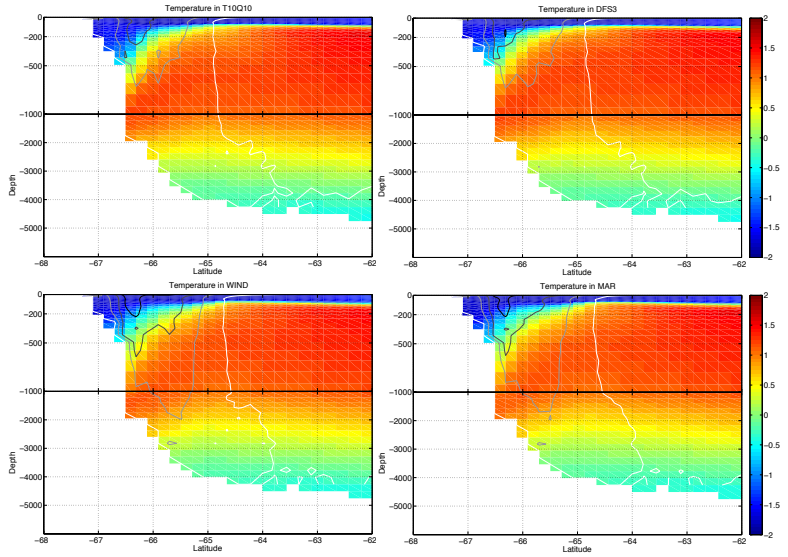

Fig. 7. Section at 60° E in simulations T10Q10, DFS3, WIND and MAR during June. Temperature is in colour and zonal currents are represented by solid lines (white is 0 cm/s, light grey is 5 cm/s, dark grey line is 10 cm/s and black line is 15 cm/s). The white area corresponds to the ocean floor. Notice that the vertical scale is not linear; a zoom is done on the first 1000 m.

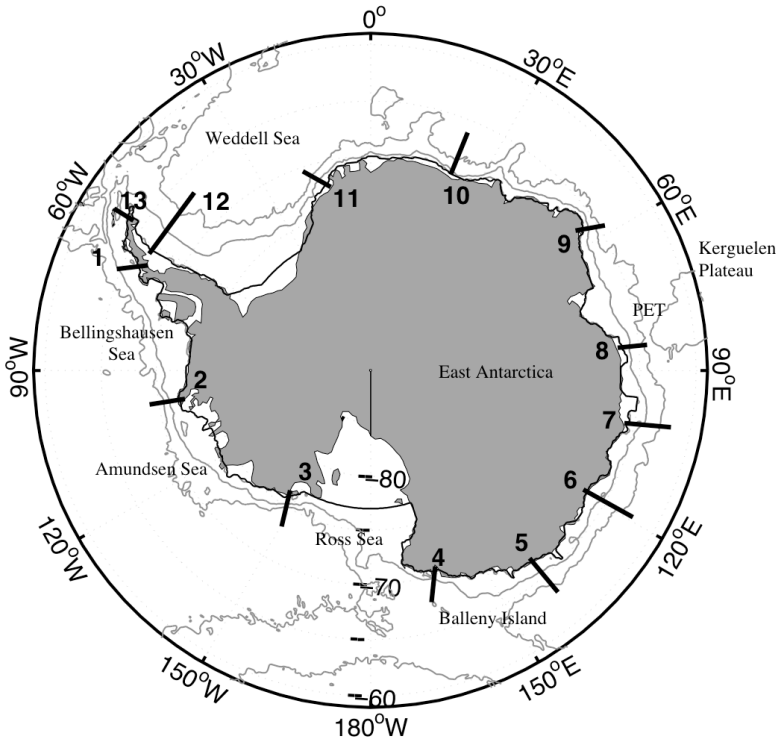

Fig. 8. Map showing all the different sections analysed in the following figures (Figs. 9–11). The grey lines correspond to bathymetry (1000 m and 3500 m). The effective offshore limit for all sections and all simulations is the 3500 m bathymetry line.

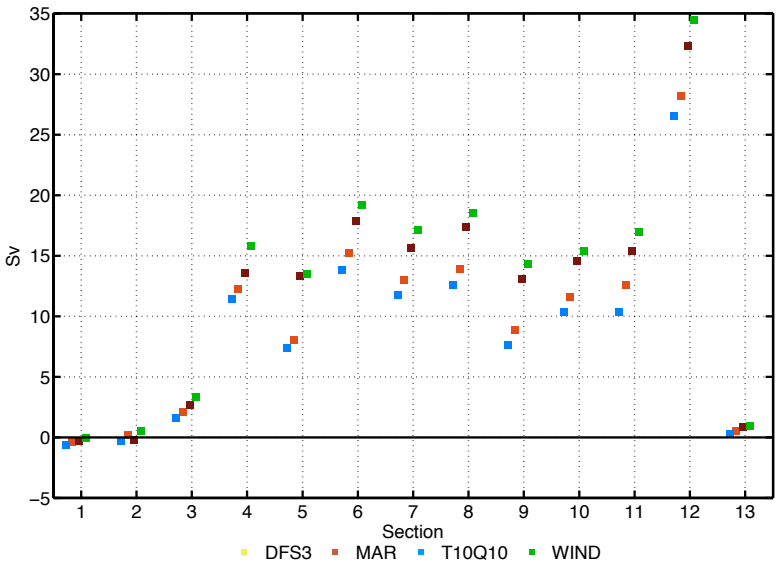

Fig. 9. Annual transport associated with the ASC in Sv across each section (horizontal axis) show in Fig. 8 for T10Q10 (blue), DFS3 (orange), MAR (brown) and WIND (green).

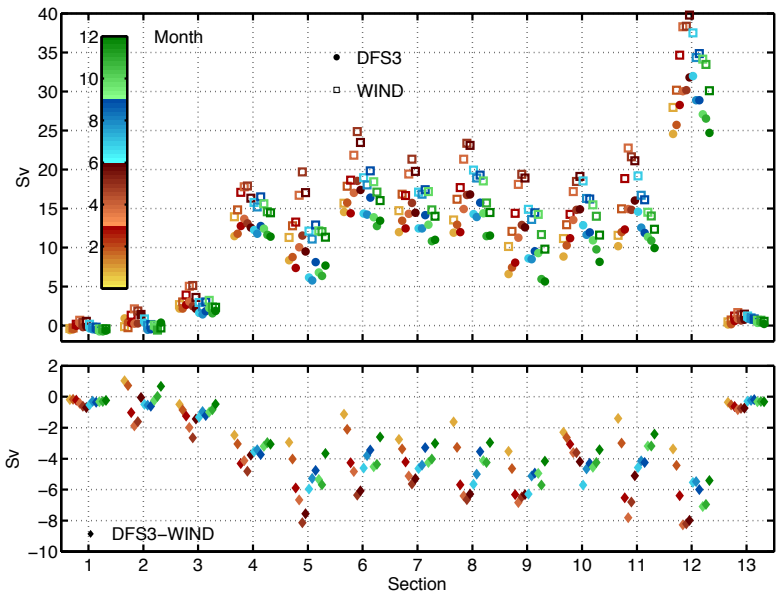

Fig. 10. Monthly ASC transport across each section (horizontal axis) shown in Fig. 8. Each number corresponds to one section, and colours correspond to the months. The upper plot represents the ASC transport. The bottom plot shows the difference between DFS3 and WIND simulations. A negative value means a stronger ASC in WIND simulation.

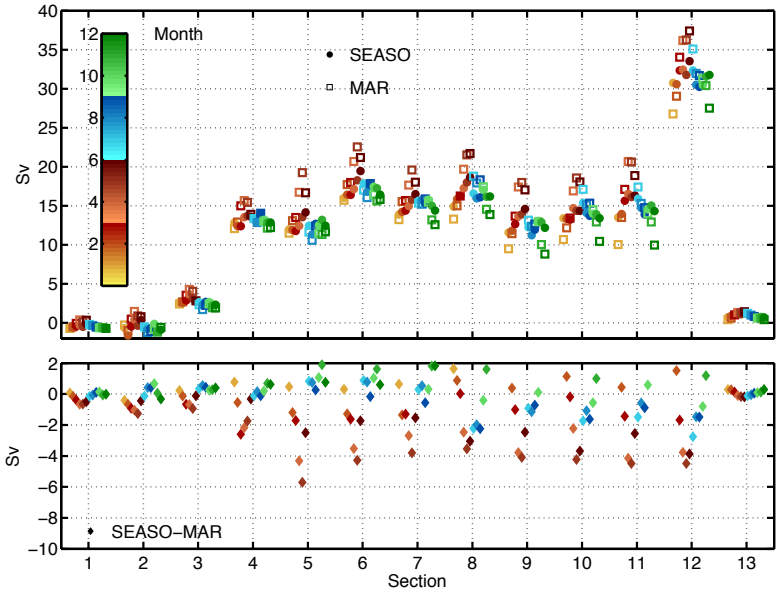

Fig. 11. Same as Fig. 10, but for SEASO and MAR simulations.

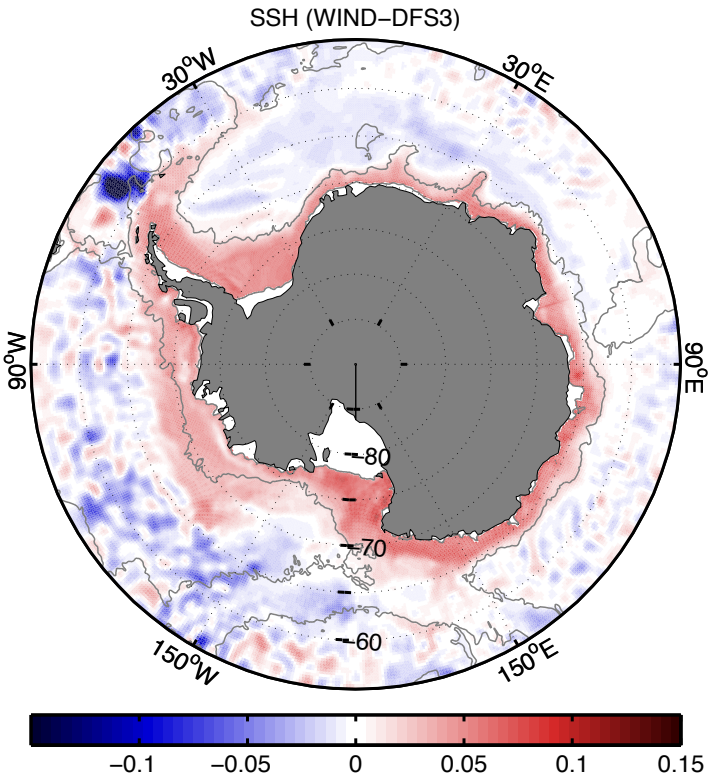

Fig. 12. SSH difference (in m) between WIND and DFS3. A red area means a higher ssh in WIND. Grey line is the 3500 m bathymetry line.

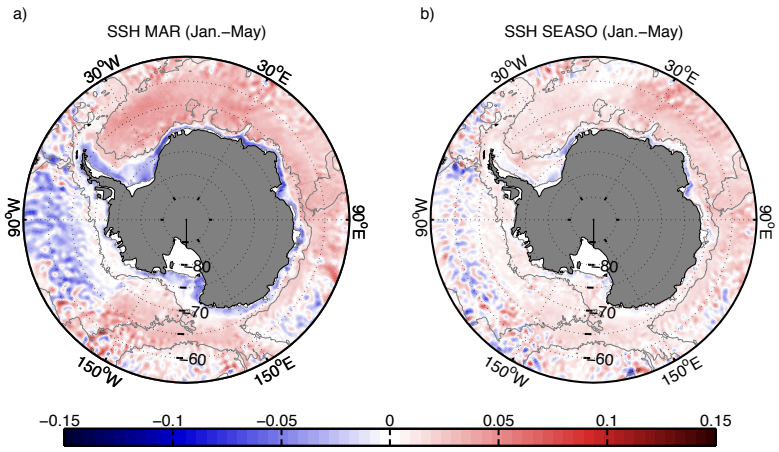

Fig. 13. SSH difference (in m) between January and May in WIND simulation **(a)** and in SEASO simulation **(b)**. A red area means a higher SSH in January. Grey line ist he 3500 m bathymetry line.